

# Atmospheric Circulation Response to an Instantaneous Doubling of Carbon Dioxide. Part I: Model Experiments and Transient Thermal Response in the Troposphere\*

YUTIAN WU

*Department of Applied Physics and Applied Mathematics, Columbia University, New York, New York*

RICHARD SEAGER, MINGFANG TING, NAOMI NAIK, AND TIFFANY A. SHAW

*Lamont-Doherty Earth Observatory, Columbia University, Palisades, New York*

(Manuscript received 24 May 2011, in final form 6 September 2011)

## ABSTRACT

This study aims to understand the dynamical mechanisms driving the changes in the general circulation of the atmosphere due to increased carbon dioxide (CO<sub>2</sub>) by looking into the transient step-by-step adjustment of the circulation. The transient atmospheric adjustment is examined using the National Center for Atmospheric Research Community Atmosphere Model, version 3, coupled to a slab ocean model, and the CO<sub>2</sub> concentration in the atmosphere is uniformly and instantaneously doubled. The thermal structure and circulation response is well established after one year of integration, with the magnitudes gradually increasing afterward toward quasi equilibrium. Tropical upper-tropospheric warming occurs in the first month. The expansion of the warming in the mid- and upper troposphere to the subtropics occurs later and is found to be primarily dynamically driven due to the intensification of transient eddy momentum flux convergence and resulting anomalous descending motion in this region. The poleward displacement of the midlatitude tropospheric jet streams occurs together with the change in eddy momentum flux convergence, but only after the intensification of the subpolar westerlies in the stratosphere. The results demonstrate the importance of the tropospheric eddies in setting up the extratropical tropospheric response to global warming.

## 1. Introduction

As the climate warms due to increased greenhouse gases in the atmosphere, the atmospheric general circulation is expected to change. Climate model simulations have found a weakening of the tropical atmospheric circulation (Held and Soden 2006; Vecchi and Soden 2007), a poleward expansion of the Hadley cell (Lu et al. 2007), a poleward shift of the tropospheric zonal jets (Kushner et al. 2001; Lorenz and DeWeaver 2007) and the midlatitude storm tracks (Yin 2005), as well as a rise in tropopause height (Kushner et al. 2001; Lorenz and DeWeaver 2007). These circulation changes have also been noticed in observational analyses for recent decades (e.g., Hu and Fu 2007; Chen and Held 2007).

Stratospheric ozone depletion in the second half of the twentieth century might dominate over the role of CO<sub>2</sub> increase in explaining Southern Hemisphere (SH) trends (Polvani et al. 2011; McLandress et al. 2011), and there is a possible contribution from natural variability in both hemispheres (e.g., Seager and Naik 2012).

Some mechanisms have been proposed to understand the cause for the extratropical circulation response to global warming. Lorenz and DeWeaver (2007) suggested that the midlatitude circulation response is predominantly driven by a rise in tropopause height based on the similarities in extratropical circulation response between a simple dry general circulation model (GCM) when the tropopause height is raised and the global warming simulations of models participating in the Coupled Model Intercomparison Project phase 3 (CMIP3) and assessed by the Intergovernmental Panel on Climate Change Fourth Assessment Report (IPCC AR4). Lu et al. (2008) proposed two possible mechanisms for the zonal mean circulation response to global warming by analyzing the CMIP3–IPCC AR4 models. The first mechanism suggests that the rising tropospheric static stability

\* Lamont-Doherty Earth Observatory Contribution Number 7516.

*Corresponding author address:* Yutian Wu, Department of Applied Physics and Applied Mathematics, Columbia University, S.W. Mudd Building, 500 West 120th Street, New York, NY 10027.  
E-mail: yw2225@columbia.edu

stabilizes the subtropical jet streams on the poleward flank of the Hadley cell, shifting the Hadley cell, the baroclinic instability zone, and the midlatitude eddies poleward. The second mechanism points to the importance of the increased phase speed of the midlatitude eddies. They suggested that the strengthened midlatitude wind in the upper troposphere and lower stratosphere, as a result of enhanced tropical upper-tropospheric warming and/or stratospheric cooling along the sloped tropopause, accelerates the eastward phase speeds of the midlatitude eddies, shifting the subtropical breaking region and the transient eddy momentum flux convergence and surface westerlies poleward. Butler et al. (2010) prescribed a heating in the tropical troposphere in a simple atmospheric GCM and found similar poleward jet and storm-track displacements as in the CMIP3–IPCC AR4 models, suggesting that the tropical upper-troposphere heating drives the circulation response to climate change. Kidston et al. (2010, 2011) found a robust increase in eddy length scale in the CMIP3–IPCC AR4 models, which is possibly caused by increased static stability in the midlatitudes. They argued that the increase in eddy length scale is a possible cause of the poleward shift of the eddy-driven jets and surface westerlies by reducing the eddy phase speed relative to the mean flow on the poleward flank of the jets and shifting the dissipation and eddy source regions poleward.

In addition, the stratosphere and its coupling with the troposphere have also been found to be important in determining the circulation response in the troposphere to global warming. Sigmond et al. (2004) studied the climate effects of middle-atmospheric and tropospheric CO<sub>2</sub> doubling separately using the ECHAM middle atmosphere climate model with prescribed sea surface temperatures (SSTs). They found strengthened Northern Hemisphere (NH) midlatitude tropospheric westerlies as a consequence of a uniform CO<sub>2</sub> doubling everywhere in the atmosphere and attributed this mainly to the middle atmosphere CO<sub>2</sub> doubling.

The mechanisms mentioned above emphasize the close link between the thermal structure and circulation responses to global warming and suggest the warming in the mid- and upper troposphere and/or the cooling in the stratosphere as possible causes. The stratospheric cooling is caused directly by increased emission due to increased CO<sub>2</sub>, while the mid- and upper-tropospheric warming in the tropics arises from increased boundary layer temperature and humidity and a shift to a warmer moist adiabatic lapse rate (e.g., Hansen et al. 1984; Held 1993). This explanation for the tropospheric warming is essentially the same as that for the enhanced tropical upper-tropospheric warming during El Niños. However, in contrast to the broad warming response under global warming, the heating in the atmosphere during El Niño

events is confined in the tropics and anomalous cooling occurs in the midlatitude troposphere induced by anomalous eddy-driven ascending motion (Seager et al. 2003). Also, the Hadley cell strengthens and narrows, and the tropospheric jets and midlatitude transient eddies shift equatorward in response to El Niños (see also Lu et al. 2008). In contrast, the warming in the mid- and upper troposphere in response to global warming, as simulated by the CMIP3–IPCC AR4 models (e.g., Fig. 10.7 in Meehl et al. 2007a), expands beyond the tropical convective region to about 40°N(S). It is not clear what causes the warming expansion into the extratropics.

In this study, we investigate the transient atmospheric adjustment to an instantaneous doubling of CO<sub>2</sub>. The response is investigated using the National Center for Atmospheric Research (NCAR) Community Atmosphere Model, version 3 (CAM3), coupled to a Slab Ocean Model (SOM). In contrast to previous studies on the equilibrium response to global warming (e.g., Hansen et al. 1984; Manabe et al. 1990; Meehl and Washington 1996; Shindell et al. 2001; Sigmond et al. 2004; Held and Soden 2006; Meehl et al. 2007a; Lu et al. 2008), our work focuses on the transient evolution that allows an assessment of the sequence of cause and effect in the circulation and thermal structure response prior to the establishment of a quasi-equilibrium state. Since the actual rate of anthropogenic CO<sub>2</sub> increase is slow compared to the instantaneous CO<sub>2</sub> doubling in our model experiments, the instantaneous CO<sub>2</sub> doubling framework may not be strictly comparable to that in the actual response to global warming in every aspect. However, we demonstrate that our simulations in both transient and equilibrium states agree well with that from the CMIP3–IPCC AR4 models in which the CO<sub>2</sub> concentration is gradually increased. Therefore, we believe that the transient atmospheric adjustment to instantaneous CO<sub>2</sub> doubling provides valuable insight into the actual mechanisms underlying the extratropical tropospheric circulation response to global warming. In the paper, the following questions will be addressed: 1) what gives rise to the broad warming in the mid- and upper troposphere between 40°S and 40°N? and 2) what are the dynamical mechanisms involved in the extratropical circulation response to increased greenhouse gases? First, we describe the model and numerical experiments in section 2. The quasi-equilibrium response in thermal structure and circulation is presented in section 3. Furthermore, section 3 also presents the transient evolution step by step, and in particular the diagnostics of the cause of the broad warming expansion in the extratropical mid- and upper troposphere. Finally, a mechanism of the extratropical tropospheric circulation response to increased CO<sub>2</sub> is proposed. Section 4 extends the analysis of the linkage

between the eddy-driven vertical motion anomaly and the warming expansion in the subtropical mid- and upper troposphere to 14 CMIP3–IPCC AR4 coupled models. Discussions and conclusions are presented in section 5. In Wu et al. (2012, manuscript submitted to *J. Climate*; hereafter Part II), we will mainly focus on the transient, sequential, response day by day before the structure of the extratropical tropospheric circulation response is established—in particular, the perturbations in both the stratosphere and the troposphere and their coupling.

## 2. Model experiments

### a. Model description

The NCAR CAM3 is a three-dimensional atmospheric general circulation model (AGCM), which includes the Community Land Model, version 3 (CLM3), an optional Slab Ocean Model, and a thermodynamic sea ice model. There are substantial modifications in the physics and dynamics of CAM3 from the previous version, Community Climate Model version 3 (CCM3), a detailed description of which is in Collins et al. (2006). CAM3 includes options for Eulerian spectral, semi-Lagrangian, and finite-volume formulations of the dynamical equations. The implementation of CAM3 with T85 spectral dynamics is the version used in the Community Climate System Model, version 3 (CCSM3), which is a fully coupled climate model for the CMIP3–IPCC AR4. CAM3 includes revised parameterizations of cloud condensation and precipitation processes as well as for radiative processes and atmospheric aerosols. The changes to the model lead to a more realistic tropical upper-troposphere temperature, a less pronounced double intertropical convergence zone, and an improved simulation of tropical continental precipitation. However, biases remain, such as the underestimation of the tropical variability associated with the Madden–Julian oscillation, the underestimation of the implied oceanic heat transport in the SH, excessive mid-latitude westerlies, and surface stress in both hemispheres (Collins et al. 2006; Hurrell et al. 2006; Rasch et al. 2006).

In this study, we use the spectral version of CAM3 with resolution T42L26 [which is equivalent to  $2.8^\circ \times 2.8^\circ$  (longitude  $\times$  latitude) horizontal resolution and 26 vertical layers with a model top at 2.917 mb] coupled to a slab ocean model and a thermodynamic sea ice model (CAM3–SOM). The slab ocean model specifies the observed climatological monthly-mean ocean mixed layer depths  $h$  and the monthly-mean distribution of the ocean heat transport  $Q_{\text{fix}}$  (“ $Q$  flux”), which is calculated from the surface energy fluxes obtained from a control run with prescribed ice and SSTs (McCaa et al. 2004; Collins et al. 2004). The mixed layer temperature (SST) is the prognostic variable computed from the slab ocean model,

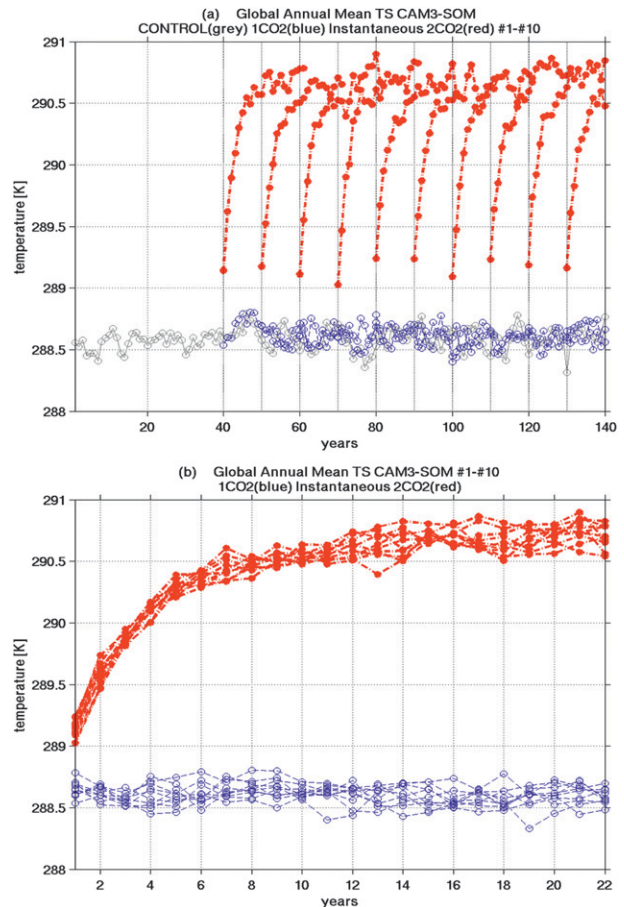


FIG. 1. (a) The global annual mean  $T_s$  for the control experiment for 140 yr (gray lines), 10 of the 100  $1\text{CO}_2$  climatological runs (each for 22 yr) (blue lines), and instantaneous  $2\text{CO}_2$  runs (each for 22 yr) (red lines). (b) As in (a), except that the time series are shifted to the same starting year (year 1) and last for 22 yr.

$$\rho_o C_p h \frac{\partial \text{SST}}{\partial t} = F_{\text{net}} + Q_{\text{fix}}, \quad (1)$$

where  $\rho_o$  and  $C_p$  are density and specific heat capacity of ocean water, respectively;  $h$  is the ocean mixed layer depth;  $F_{\text{net}}$  is the net surface energy flux from the atmosphere to the ocean; and  $Q_{\text{fix}}$  is the prescribed ocean heat transport.

### b. Experimental design

A control experiment of CAM3–SOM is run for 140 yr with the  $\text{CO}_2$  concentration fixed at 355 ppmv. The year-by-year evolution of the global annual mean surface temperature ( $T_s$ ) is shown in Fig. 1a (gray line) and has an average value of 288.5 K. The model asymptotes toward a quasi-equilibrium state after approximately 20 years (not shown).

Using 1 January of each year of the last 100 yr of the control experiment as initial conditions, we generated a 100-member ensemble of single- and doubled- $\text{CO}_2$  pair runs ( $1\text{CO}_2$  and  $2\text{CO}_2$ , respectively). The  $1\text{CO}_2$  run is the

same as the control experiment and keeps the CO<sub>2</sub> level constant at 355 ppmv and is integrated forward for 22 yr. The 2CO<sub>2</sub> experiment is a branch model run lasting for 22 yr as well and doubles the CO<sub>2</sub> concentration instantaneously to 710 ppmv at the beginning of the experiment on 1 January. The difference between the 1CO<sub>2</sub> run and the instantaneous 2CO<sub>2</sub> run provides the atmospheric response to an instantaneous doubling of CO<sub>2</sub>. The ensemble average across the 100 runs to a large extent removes the model's internal variability and allows for an assessment of the day-to-day adjustment of the atmospheric general circulation. Several variables, such as zonal and meridional winds, temperature and specific humidity, are output daily for the first 2 yr of the model integration. This methodology has been applied successfully to the study of cause and effect in the tropospheric response to El Niño and tropical Atlantic SST anomalies (Seager et al. 2009, 2010a,b; Harnik et al. 2010).

### 3. Results

#### a. Global mean response

Figure 1 shows the year-by-year evolution of the global annual mean  $T_s$  for the 1CO<sub>2</sub> runs (blue lines) and the 2CO<sub>2</sub> runs (red lines) for 10 of the 100 ensemble runs. The global annual mean  $T_s$  immediately increases by about 0.5 K in the first year after the doubling of CO<sub>2</sub> on 1 January. After about 20 years, the 2CO<sub>2</sub> runs reach a quasi-equilibrium state with  $T_s$  asymptoting toward an increase of 2.2 K (shown in Figs. 1a and 1b).

The CO<sub>2</sub> forcing and the model's climate sensitivity are also examined in the 2CO<sub>2</sub> runs. Following Gregory et al. (2004), a scatterplot of the ensemble mean change in global annual mean  $T_s$  and the change in global annual mean net radiative flux at the top of the atmosphere (TOA) for the 22 yr of integration is shown in Fig. 2. The intercept of the regression line provides an estimate for the CO<sub>2</sub> forcing at the time of doubling,  $F_{2\times} = 3.33 \text{ W m}^{-2}$ , and the slope indicates the climate response parameter  $\alpha = 1.54 \text{ W m}^{-2} \text{ K}^{-1}$ . In Gregory and Webb (2008), they found a doubled CO<sub>2</sub> forcing of  $2.93 \pm 0.23 \text{ W m}^{-2}$  and a climate feedback parameter of  $1.1 \text{ W m}^{-2} \text{ K}^{-1}$  for the CCSM3 T85 slab ocean model. The two results generally agree with each other despite different horizontal resolutions.

#### b. Equilibrium response

As shown in Fig. 1, the 2CO<sub>2</sub> simulations reach equilibrium after about 20 years. Figure 3 shows the equilibrium response in zonal mean temperature ( $T$ ), zonal wind ( $u$ ), transient eddy momentum flux ( $\langle \overline{u'v'} \rangle = \langle \overline{uv} \rangle - \langle \overline{u} \overline{v} \rangle$ ),

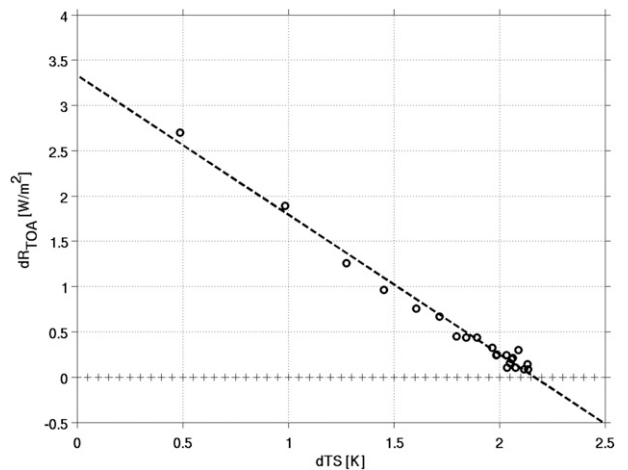


FIG. 2. Scatterplot of the year-to-year change in global annual mean  $T_s$  and net radiative flux at TOA for the 22 yr of 2CO<sub>2</sub> integration. It provides an estimate for the doubling CO<sub>2</sub> forcing  $F_{2\times} = 3.33 \text{ W m}^{-2}$  and the climate sensitivity of about 2.2 K.

and variance of transient meridional velocity ( $\langle \overline{v'v'} \rangle = \langle \overline{v^2} \rangle - \langle \overline{v} \overline{v} \rangle$ ) averaged over 100 ensemble members in year 22 for January–March (JFM) and June–August (JJA), where bars denote monthly averages, primes denote deviations from monthly averages, and angle brackets denote zonal averages. The colors show the difference between the 2CO<sub>2</sub> runs and the 1CO<sub>2</sub> runs, and the contours show the climatological response from the 1CO<sub>2</sub> runs. The 95% significance level among the 100 ensemble runs is plotted with gray dots. We also estimated the tropopause height as the lowest pressure level at which the temperature lapse rate decreases to  $2 \text{ K km}^{-1}$  following the algorithm in Reichler et al. (2003). Figure 3a shows the tropopause level for the 1CO<sub>2</sub> (2CO<sub>2</sub>) runs in green (dashed magenta) lines. As expected, the troposphere warms everywhere with a maximum in the tropical upper troposphere, and the stratosphere cools due to additional radiation emission to space. The tropopause height associated with the temperature increase (decrease) in the troposphere (stratosphere) rises by about 5–10 mb in the tropics and 10–20 mb in the extratropics, which is broadly consistent with Lu et al. (2008). The zonal mean zonal wind response shows a prominent acceleration in the upper troposphere and the stratosphere in both seasons and both hemispheres with the exception of a strong reduction in the stratospheric polar jet in JJA in the SH. The zonal wind response in the mid- and lower troposphere is less obvious, but in the SH there is a clear poleward shift in the tropospheric jet streams and an intensification of about  $0.5 \text{ m s}^{-1}$  on the poleward side of the climatological jets. In the NH, there is a weak poleward shift. These features in the equilibrium zonal wind response are also true for the NCAR CCSM3 coupled model simulations (not shown).

<sup>1</sup> Without bandpass filtering.

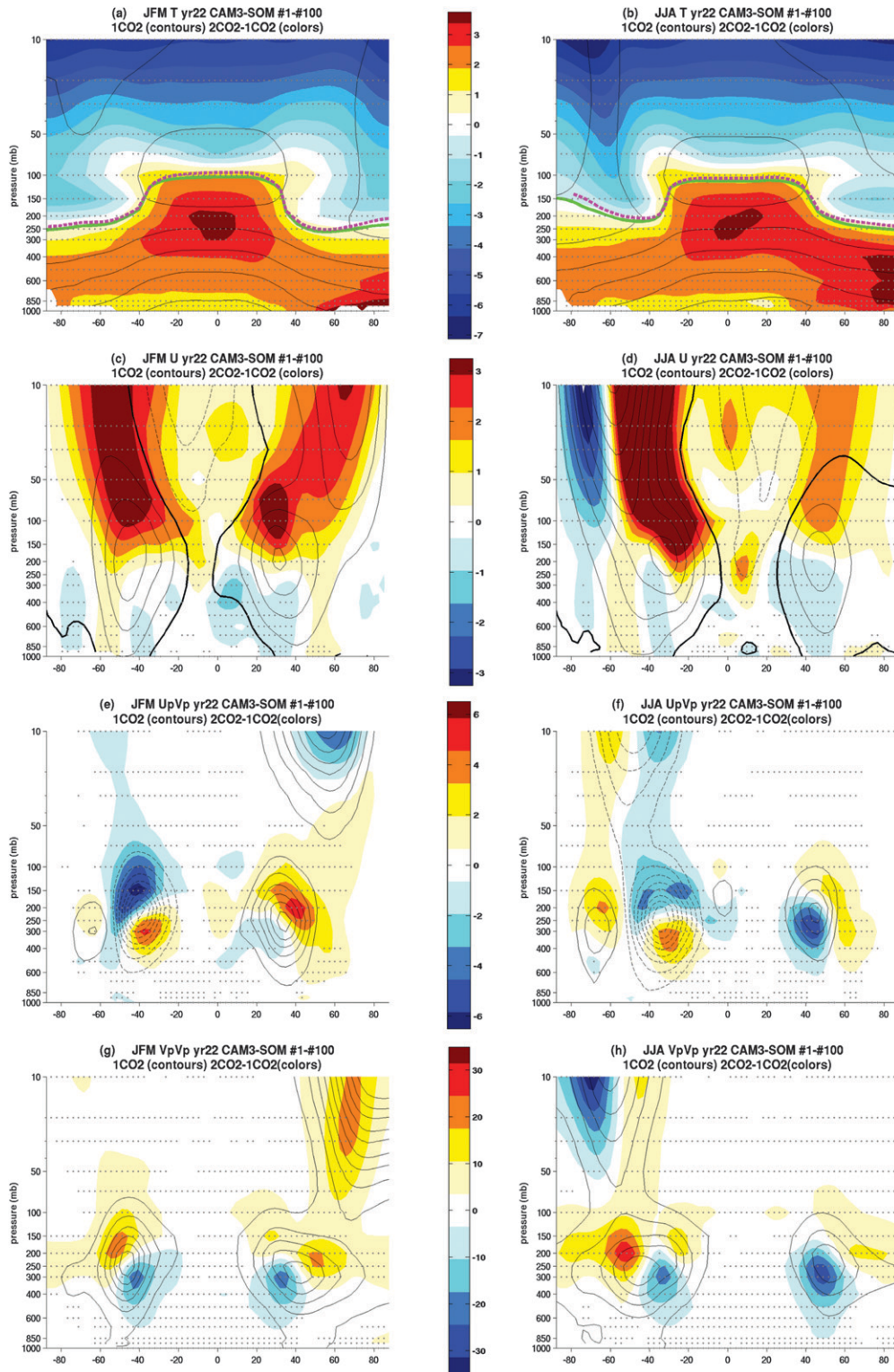


FIG. 3. The  $2\text{CO}_2$  equilibrium response in (a),(b)  $\langle T \rangle$ , (c),(d)  $\langle \bar{u} \rangle$ , (e),(f)  $\langle \bar{u}'v' \rangle$ , and (g),(h)  $\langle \bar{v}'v' \rangle$  for (left) JFM and (right) JJA as a function of latitude and pressure level. The tropopause level is plotted in green (dashed magenta) lines for the  $1\text{CO}_2$  ( $2\text{CO}_2$ ) runs. The colors show the difference between the  $2\text{CO}_2$  and the  $1\text{CO}_2$  runs, while the contours show the climatology. The thick black lines in (c),(d) denote the climatological zero wind lines. The gray dots indicate the 95% significance level for the responses. The contour intervals are (a),(b) 20 K, (c),(d) 10  $\text{m s}^{-1}$ , (e),(f) 10  $\text{m}^2 \text{s}^{-2}$ , and (g),(h) 50  $\text{m}^2 \text{s}^{-2}$ .

The responses in transient eddy momentum flux and variance of meridional velocity include a prominent poleward and upward shift, especially in the upper troposphere and lower stratosphere. There is also an intensification in  $\langle \overline{u'v'} \rangle$  on the poleward side of the climatological maxima (NH) and minima (SH), which agrees well with that simulated in the CMIP3–IPCC AR4 coupled models (e.g., Lu et al. 2008; Wu et al. 2010). The change in  $\langle \overline{v'v'} \rangle^2$  is also broadly consistent with that simulated in the CMIP3–IPCC AR4 models (e.g., Yin 2005; Wu et al. 2010; O’Gorman 2010), except the areas of reduction in  $\langle \overline{v'v'} \rangle$  on the equatorward flank of the climatological maxima are more pronounced in our experiments.

The response in transient eddies agrees well with the temperature anomaly and the change in linear baroclinic instability in CAM3–SOM. The largest increase in meridional temperature gradient occurs in the midlatitude upper troposphere and lower stratosphere. This is consistent with the strengthened transient eddies in this region. The close linkage between the thermal structure change and the circulation response to increased greenhouse gases has also been found in other studies (e.g., Yin 2005; Wu et al. 2010; O’Gorman 2010; Butler et al. 2010). Because neither daily variables nor monthly covariances in the NCAR CCSM3 coupled model are available for the CMIP3–IPCC AR4 experiments, the transient eddy activity and its future projections in the coupled model cannot be assessed and compared with our results.

### c. Transient atmospheric adjustment and thermodynamics

#### 1) TRANSIENT RESPONSE

Figures 4–6 show the month-by-month evolution of  $\langle \overline{T} \rangle$ ,  $\langle \overline{u} \rangle$ , and  $\langle \overline{u'v'} \rangle$  during the first year after the CO<sub>2</sub> concentration is instantaneously doubled on 1 January. The temperature structure and circulation response in the atmosphere are well established during the first year. For example, the pattern correlation between years 1 and 22 in  $\langle \overline{u} \rangle$  is above 0.6 for all months (not shown). The stratospheric cooling in December of year 1 is already similar to that of the equilibrium response (shown in Fig. 3a). The tropospheric temperature adjustment also resembles that in equilibrium with a prominent warming in the tropical mid- and upper troposphere, albeit with lesser magnitude. The stratosphere responds to the CO<sub>2</sub> doubling almost instantaneously and cools by about 2 K in January. The response in the troposphere is slower

because of the delay associated with the warming of the oceans followed by transmission of the warming into the troposphere. The mid- and upper troposphere in the extratropics only warms up by about 0.5 K in March. The change in tropopause height is quite small in year 1, with the climatological 1CO<sub>2</sub> run and 2CO<sub>2</sub> run tropopause heights basically overlapping. The tropopause level, in general, rises by about 2 mb, except for about 10 mb in the NH high latitudes in March of year 1. In March there is also a large westerly anomaly in the stratosphere in both hemispheres and the tropospheric zonal jets shift poleward. This then persists in the SH but weakens probably due to seasonal variation in the NH.<sup>3</sup> The response in transient eddy momentum flux in the troposphere gets stronger on the poleward side of the climatological jets starting from March of year 1. Similar to the change in tropospheric jets, the strengthening of the transient eddies occurs persistently throughout the year in the SH but has a notable seasonal variation in the NH.

Figures 7a and 7b show the day-by-day evolution of the zonal mean temperature and zonal wind averaged over 30°–70°N from 1 January 1 to 30 April 30 of year 1 as a function of time and pressure level. The average over 30°–70°S is shown in Figs. 7c and 7d. The response is robust for different choices of latitudinal bands. A 5-day running average has been applied to all the variables. It is noted that the cooling in the stratosphere occurs first in the upper stratosphere and extends to the lower stratosphere in about a month. The substantial warming (0.5 K) in the mid- and upper troposphere takes place in early March. The eastward zonal wind anomaly clearly begins in the upper stratosphere and then gradually moves downward into the lower stratosphere and the troposphere, with the whole process taking about 100 days. The succession of events, first happening in the stratosphere and subsequently in the troposphere, resembles that in observations of subseasonal to seasonal variability (Baldwin and Dunkerton 2001) as well as in the “downward control” theory (Haynes et al. 1991).

Figure 8 shows the day-by-day response in  $\langle \overline{T} \rangle$ ,  $\langle \overline{u} \rangle$ , total, and 2–8-day bandpass-filtered<sup>4</sup> eddy momentum flux convergence as a function of time and latitude in January–April (JFMA) of year 1. These variables are all averaged

<sup>3</sup> In this model experiment, the NH tropospheric jet shift in summer is very weak (in both the transient and equilibrium states), while that in winter is slightly stronger (shown in Figs. 3c and 3d). However, there is not much seasonal dependence for the tropospheric jet displacement in the SH.

<sup>4</sup> The time filter used here is a standard 21-point two-sided bandpass filter that keeps the variability within 2–8 days. It skips the first and last 10 days in the time series of daily eddy momentum flux convergence.

<sup>2</sup> The change in  $\langle \overline{v'v'} \rangle$  is similar to the result after a bandpass filter that retains synoptic variability within 2–8 days (not shown).

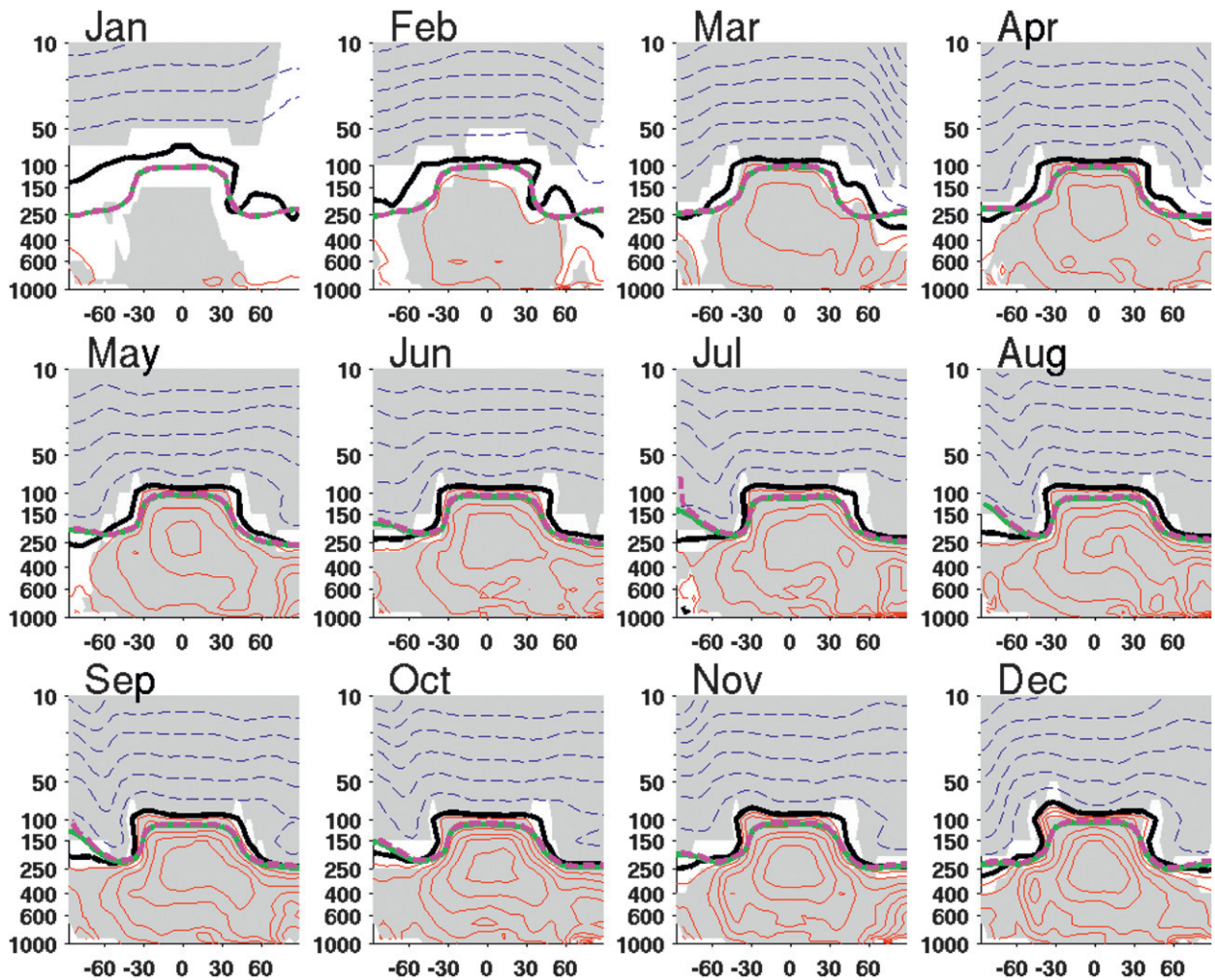


FIG. 4. The month-by-month transient response in  $\langle \bar{T} \rangle$  in year 1 shown as a function of latitude and pressure level. The color contours show the difference between the 2CO<sub>2</sub> and the 1CO<sub>2</sub> runs with red (dashed blue) denoting positive (negative) anomalies. The thick black lines show zero values. The tropopause height is plotted in thick green (dashed magenta) lines for the 1CO<sub>2</sub> (2CO<sub>2</sub>) runs. The gray shadings show the 95% significance level. The contour intervals are 0.25 K for positive values and  $-1$  K for negative values.

over the mid- and upper troposphere from 150 to 500 mb, and a two-dimensional spatial (latitude–pressure level) 1–2–1 smoothing and a 10-day temporal running average are applied in plotting. Gray shadings in Fig. 8 denote the 90% significance level among the 100 ensemble runs. The total eddy momentum flux convergence is defined as  $-(1/a \cos^2 \phi) [\partial \langle uw \rangle - \langle u \rangle \langle v \rangle \cos^2 \phi / \partial \phi]$ , while its bandpass-filtered transient component is denoted as  $-(1/a \cos^2 \phi) [\partial \langle u_H v_H \rangle \cos^2 \phi / \partial \phi]$ . As shown in Fig. 8a, the warming of the mid- and upper troposphere first occurs in the tropics and then extends to the subtropics around and beyond 40°S in mid-February and 40°N in early March. Almost simultaneously the jet in the mid- and upper troposphere is displaced poleward with a reduction in zonal wind equatorward of 40°N and an intensification poleward of 40°N and 40°S (shown in Fig. 8b).

The change in eddy momentum flux convergence, and in particular its bandpass-filtered component, shows a similar transition, with a dipole pattern starting from mid-February in the SH and early March for the NH (shown in Figs. 8c and 8d). In fact, this (significant) enhanced transient eddy momentum flux convergence in the extratropics occurs ahead of the (significant) tropospheric jet shift and acts to accelerate the westerlies in the subtropical mid- and upper troposphere.

## 2) THERMODYNAMIC DIAGNOSTICS

As mentioned in the introduction, there is a close link and consistency between the tropospheric thermal structure and the circulation response in both the El Niños and the global warming scenario. During the El Niños, there is a confined tropical tropospheric warming and a cooling in

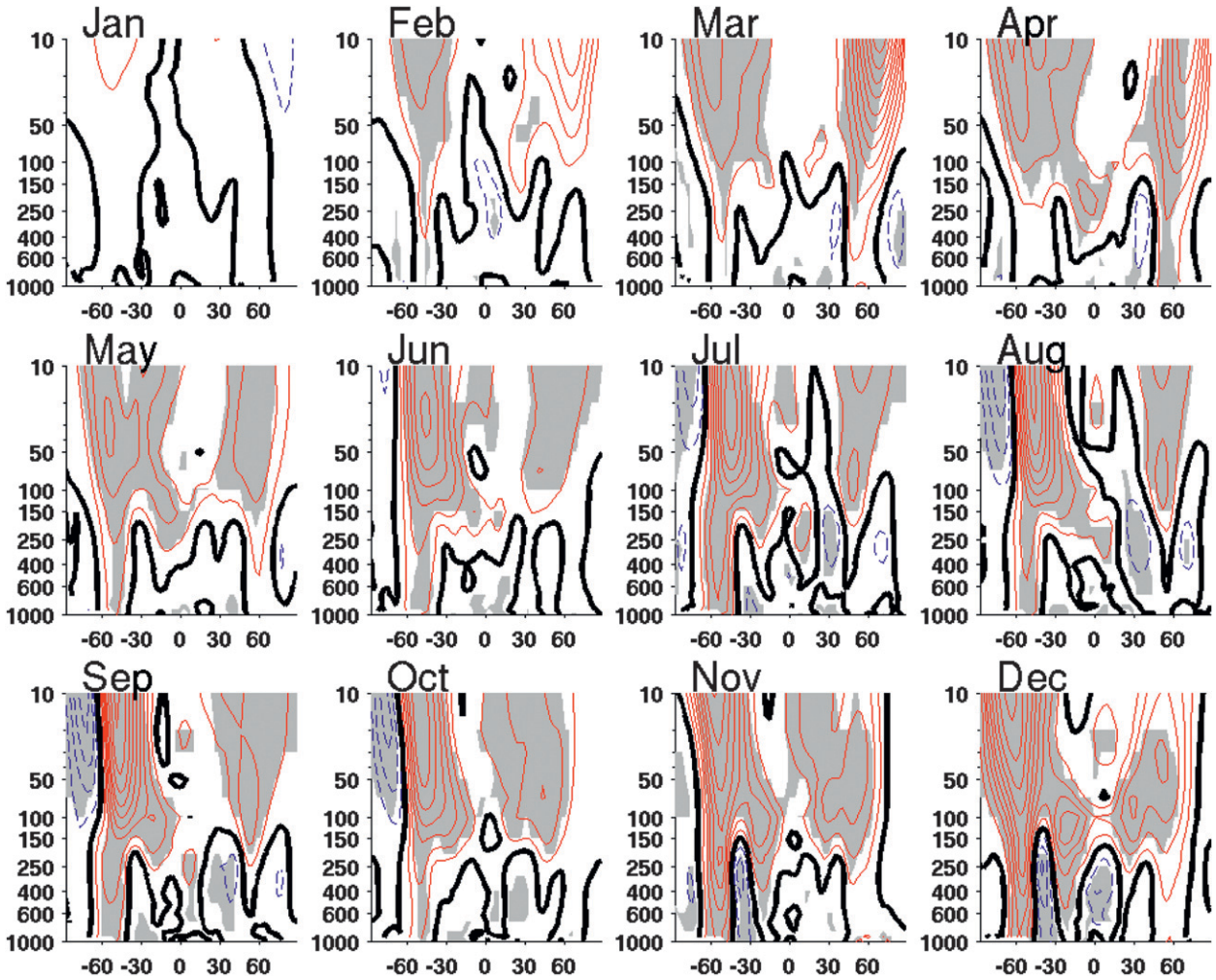


FIG. 5. As in Fig. 4, but for  $\langle \bar{v} \rangle$ . The contour interval is  $0.5 \text{ m s}^{-1}$ .

the midlatitudes that is associated with an equatorward displacement of the tropospheric jets and midlatitude transient eddies. In contrast, as a result of the  $\text{CO}_2$  increase, the tropospheric warming extends broadly into the subtropics and the midlatitudes along with a poleward shift of the zonal wind and the storm tracks. Previous studies have demonstrated that the midlatitude cooling in response to the El Niños is driven by eddy-induced ascent anomaly (Seager et al. 2009, 2010a,b; Harnik et al. 2010).

Therefore, what is responsible for the extensive tropospheric warming to  $\text{CO}_2$  increase?

This section will diagnose the cause of the subtropical warming tendency (diabatic vs adiabatic) in the  $2\text{CO}_2$  experiments. Here we focus on March of year 1, when the mid- and upper troposphere starts to warm up in the NH subtropics by about  $0.5 \text{ K}$  (shown in Fig. 4). Following Seager et al. (2003), the zonal mean temperature budget is written as

$$\begin{aligned}
 \frac{\partial \langle \bar{T} \rangle}{\partial t} = & \underbrace{- \left[ \frac{\langle \bar{v} \rangle}{a} \frac{\partial \langle \bar{T} \rangle}{\partial \phi} + \langle \bar{\omega} \rangle \left( \frac{\partial \langle \bar{T} \rangle}{\partial p} - \frac{R \langle \bar{T} \rangle}{C_p p} \right) \right]}_{\text{(a) MMC}} \\
 & - \underbrace{\frac{1}{a \cos \phi} \frac{\partial}{\partial \phi} [(\langle \bar{v} \bar{T} \rangle - \langle \bar{v} \rangle \langle \bar{T} \rangle) \cos \phi]}_{\text{(b) Eddies}} - \frac{\partial}{\partial p} (\langle \bar{\omega} \bar{T} \rangle - \langle \bar{\omega} \rangle \langle \bar{T} \rangle) + \frac{R}{C_p} \frac{1}{p} (\langle \bar{\omega} \bar{T} \rangle - \langle \bar{\omega} \rangle \langle \bar{T} \rangle) + \underbrace{\frac{\langle \bar{Q} \rangle}{C_p}}_{\text{(c) Diabatic Heating}}, \quad (2)
 \end{aligned}$$

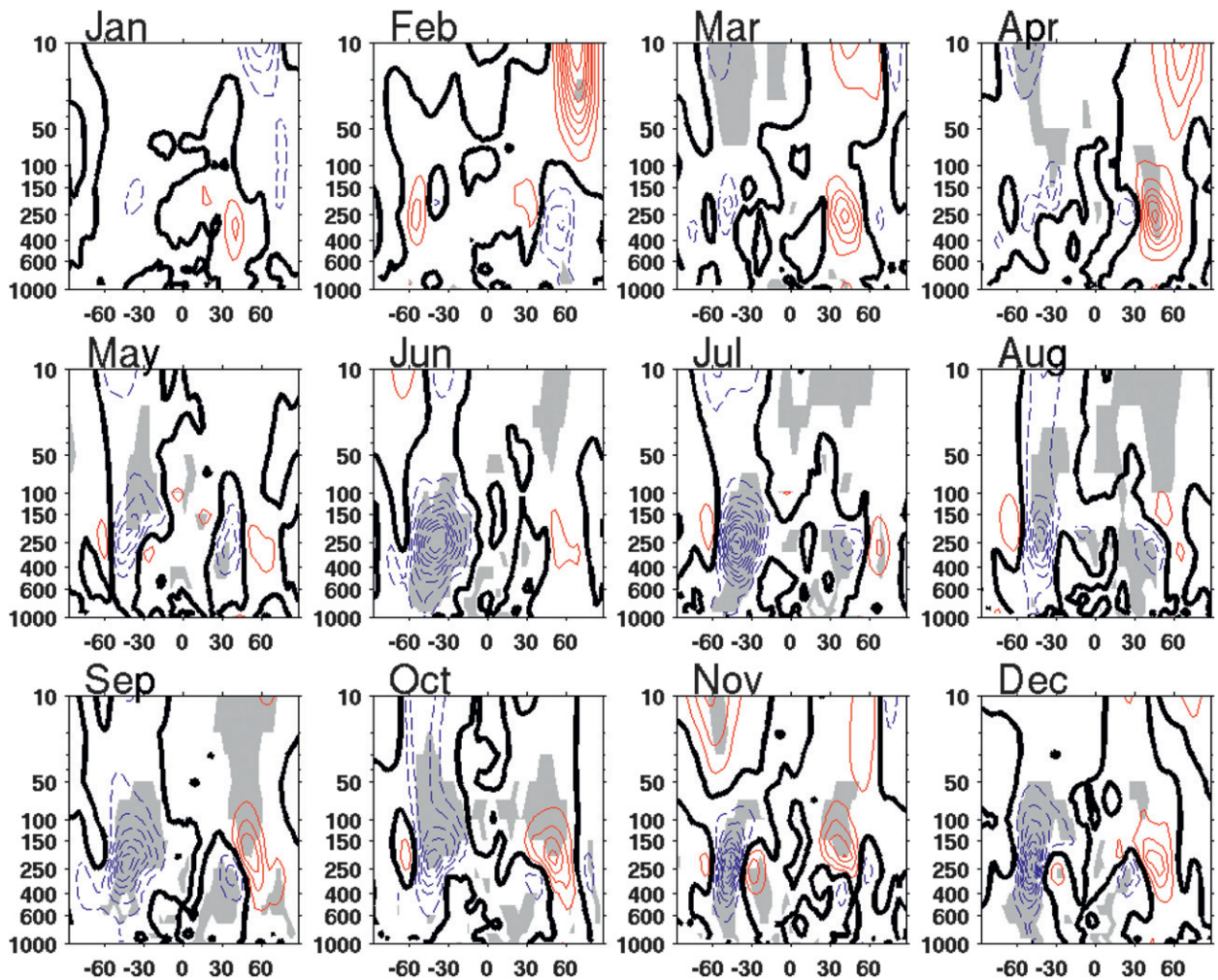


FIG. 6. As in Fig. 4, but for  $\langle u'v' \rangle$ . The contour interval is  $1 \text{ m}^2 \text{ s}^{-2}$ .

where bars denote monthly averages and brackets denote zonal averages. In Eq. (2), the temperature tendency is divided into contributions from 1) the mean meridional circulation (MMC), 2) the transient and stationary eddies, and 3) the total diabatic heating  $Q$ . The diabatic heating term is the sum of the temperature tendency due to horizontal diffusion and vertical diffusion, solar heating rate, longwave heating rate, and the heating resulting from shallow, deep-convective, and large-scale condensation processes. Other terms, such as the temperature tendency due to orographic gravity wave drag and kinetic energy (KE) dissipation, are not saved and are neglected in our analysis. However, because of the reformulation of the parameterized heating since CAM2 to conserve energy in the model, the KE dissipation term in the surface layer is large ( $\approx 0.9 \text{ K day}^{-1}$ ) and maximizes in the midlatitude oceanic storm-track region where the surface stress is large (Boville and Bretherton 2003). This KE dissipation term results in

some discrepancies in the balance in the zonal mean temperature equation in the surface layer (not shown).

Figure 9 shows the latitude–pressure level plot of the net temperature tendency ( $\partial\langle T \rangle/\partial t$ ) (Fig. 9a), the temperature tendency computed from the rhs of Eq. (2) (Fig. 9b), the temperature tendencies due to the MMC (Fig. 9c), the eddies (Fig. 9d), and the total diabatic heating (Fig. 9f), separately, during March of year 1. In addition, Fig. 9e shows the total dynamical contribution, computed as the sum of the MMC and the eddies (Figs. 9c and 9d, respectively). The colors show the difference between the  $2\text{CO}_2$  runs and the  $1\text{CO}_2$  runs, and the contours show the results from the  $1\text{CO}_2$  runs. The net temperature tendency (in units of  $\text{K month}^{-1}$ ) is estimated as the temperature difference from 1 to 31 March, which shows a warming tendency in the subtropical mid- and upper troposphere from 200 to 500 mb and from  $20^\circ$  to  $45^\circ\text{N}$  (indicated by the black box in Fig. 9) as well as a warming tendency poleward of  $50^\circ\text{N}$ . Figure 9b, in colors,

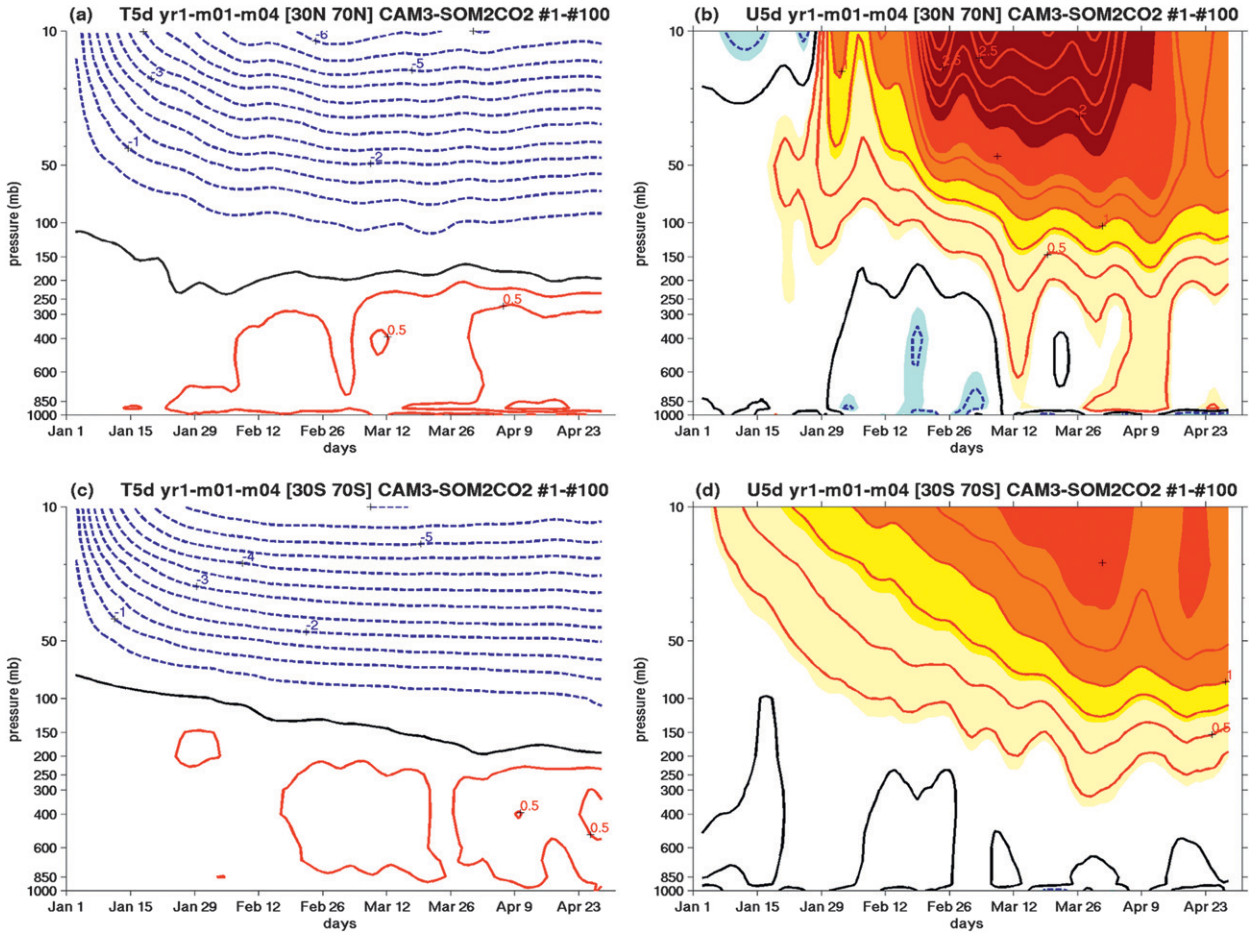


FIG. 7. The  $2\text{CO}_2$  transient day-by-day response in (a),(c)  $\langle T \rangle$  and (b),(d)  $\langle u \rangle$  shown as a function of day (from 1 Jan to 30 Apr) and pressure level averaged between (a),(b)  $30^\circ$  and  $70^\circ\text{N}$ , and (c),(d)  $30^\circ$  and  $70^\circ\text{S}$ . A 5-day running average has been applied for plotting. The contour intervals are  $0.25\text{ K}$  ( $-0.5\text{ K}$ ) for positive (negative) values in (a),(c) and  $0.25\text{ m s}^{-1}$  for (b),(d).

shows the matching temperature tendency computed from the rhs of Eq. (2), which, away from the surface, is in good agreement with the actual tendency shown in Fig. 9a. A comparison between Figs. 9e and 9f shows that the thermodynamical and dynamical contributions are always opposing each other, and it is the dynamical part that leads to the warming tendency in the subtropical mid- and upper troposphere. More specifically, the adiabatic warming in the subtropical mid- and upper troposphere comes from the change in MMC, which is mostly attributed to the anomalous downward vertical motion (Fig. 9c) and is opposed by the change in transient eddy heat transport (Fig. 9d) and, at lower levels, diabatic heating (Fig. 9f). The anomalous downward vertical motion in the subtropical region, in fact, tends to reduce the low-level cloud cover and the condensational heating rate (not shown)

and, hence, the total diabatic heating in the region. The polar warming at northern high latitudes is caused by the increased diabatic heating, in particular, the increased longwave radiative heating as a result of increased greenhouse gases (Fig. 9f). The temperature tendency diagnosis demonstrates that the warming expansion beyond the tropical convective region is mainly dynamically driven and thermodynamically opposed with the circulation change preceding the tropospheric temperature change.

To identify the cause for the anomalous vertical motion in the subtropics, we have computed the eddy-driven vertical motion  $\omega_{\text{eddy}}$ . It is derived using the continuity equation and the balance between the Coriolis torque and the momentum flux convergence, which is the dominant balance in the extratropics in the zonal momentum equation, following Seager et al. (2003), as shown:

$$\langle \bar{\omega}_{\text{eddy}}(p) \rangle = \langle \bar{\omega}(p_o) \rangle - \frac{1}{a \cos \phi} \frac{\partial}{\partial \phi} \times \int_{p_o}^p \frac{1}{a \cos \phi f} + \frac{1}{a^{-1} \langle \bar{u} \rangle \tan \phi} \frac{\partial}{\partial \phi} (\langle \bar{u}'v' \rangle \cos^2 \phi) dp, \quad (3)$$

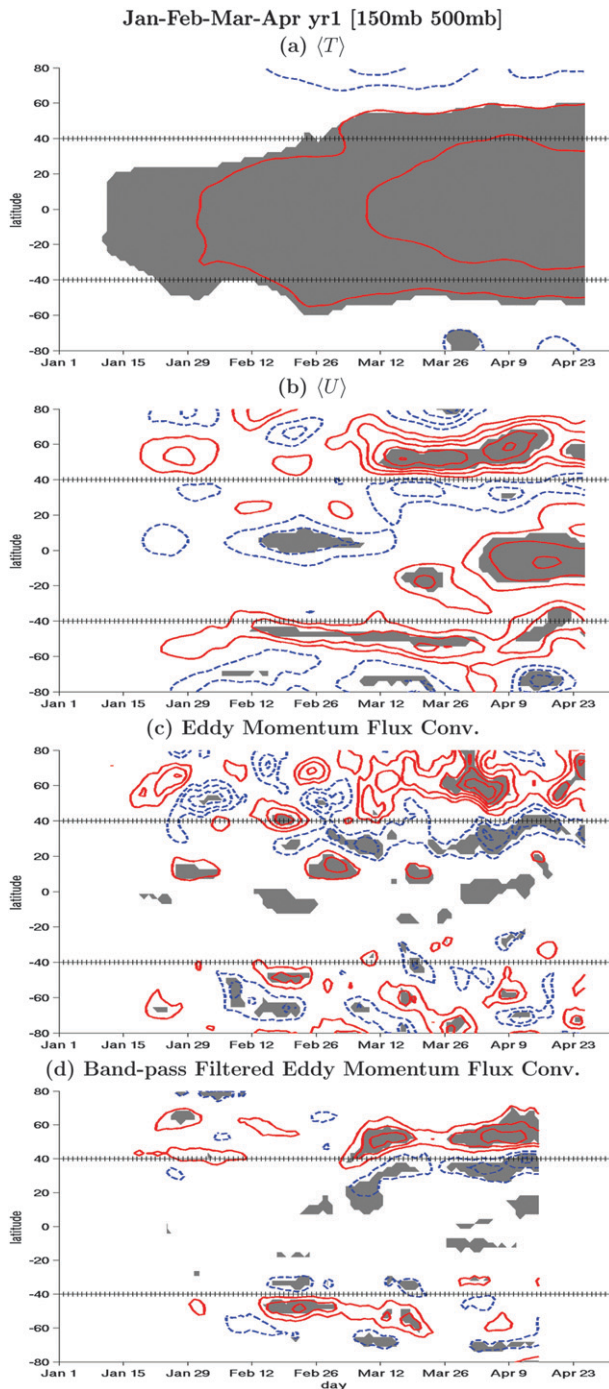


FIG. 8. The  $2\text{CO}_2$  transient day-by-day response in (a)  $\langle T \rangle$ , (b)  $\langle u \rangle$ , (c) total, and (d) bandpass-filtered eddy momentum flux convergence (defined in text) as a function of day (from 1 Jan to 30 Apr) and latitude. These variables are averaged from 150 to 500 mb, and a two-dimensional (latitude–pressure level) 1–2–1 smoothing and a 10-day temporal running average are applied. Gray shadings denote the 90% significance level. The contour intervals are (a) 0.25 K, (b)  $0.25 \text{ m s}^{-1}$ , and (c),(d)  $0.1 \text{ m s}^{-1} \text{ day}^{-1}$ .

where  $p_o$  is taken to be  $100 \text{ mb}^5$  [Eq. (3) is not applicable in the deep tropics where the Coriolis parameter approaches zero]. This is, in fact, the downward motion controlled by the wave forcing above in the “downward control” principle in Haynes et al. (1991), except in the conventional Eulerian framework. The eddy-induced motion  $\omega_{\text{eddy}}$  was computed at all pressure levels using  $\langle \bar{u} \rangle$  and  $\langle u'v' \rangle$  from the model output. Figure 10 shows  $\omega_{\text{eddy}}$  computed from Eq. (3) and the actual vertical motion  $\omega$  from the model output in March of year 1 (notice that the values of  $\omega_{\text{eddy}}$  are large in the surface layer because of neglect of surface friction). In both hemispheres there is reasonable agreement in the meridional structure of the actual vertical velocity and the eddy-induced vertical velocity away from the tropics in both the climatological  $1\text{CO}_2$  runs (shown in contours) and the  $2\text{CO}_2$  run anomalies (shown in colors). The anomaly in  $\omega_{\text{eddy}}$  is primarily attributed to the change in  $\langle u'v' \rangle$ . As shown in Fig. 10b, there is an anomalous ascending motion in the NH tropics driven by enhanced tropical convective heating following the  $\text{CO}_2$  increase that is consistent with the increased diabatic heating in the region (Fig. 9f). In the NH subtropics (between  $30^\circ$  and  $45^\circ\text{N}$ ), there is a descending motion anomaly that also shows up in the change in  $\omega_{\text{eddy}}$ . This indicates that the anomalous downward motion is primarily driven by the enhanced transient eddy momentum flux convergence. The Hadley cell expansion as found in CMIP3–IPCC AR4 coupled models (Lu et al. 2007) is also presumably related to the changing transient eddies in this region.

As shown in Fig. 8a, the subtropical warming expansion in the SH takes place in mid-February of year 1, albeit of small magnitude. A similar thermodynamic analysis has been done for February, and it is found that the SH subtropical warming at that time is also driven by enhanced transient eddy momentum flux convergence and resulting anomalous downward vertical motion (not shown).

The heating anomaly in the subtropical mid- and upper troposphere in this model experiment is induced by the dynamical circulation change rather than vice versa. It is the enhanced transient eddy momentum flux convergence in response to increased  $\text{CO}_2$  that causes anomalous descending motion and adiabatic heating in the subtropical mid- and upper troposphere. The dynamics of the changing transient eddies is closely connected with the response in the stratosphere and coupling between the stratosphere and the troposphere, and this will be further investigated in Part II.

<sup>5</sup> There is a  $\cos\phi$  term missing in the denominator of Eq. (7) in Seager et al. (2003).

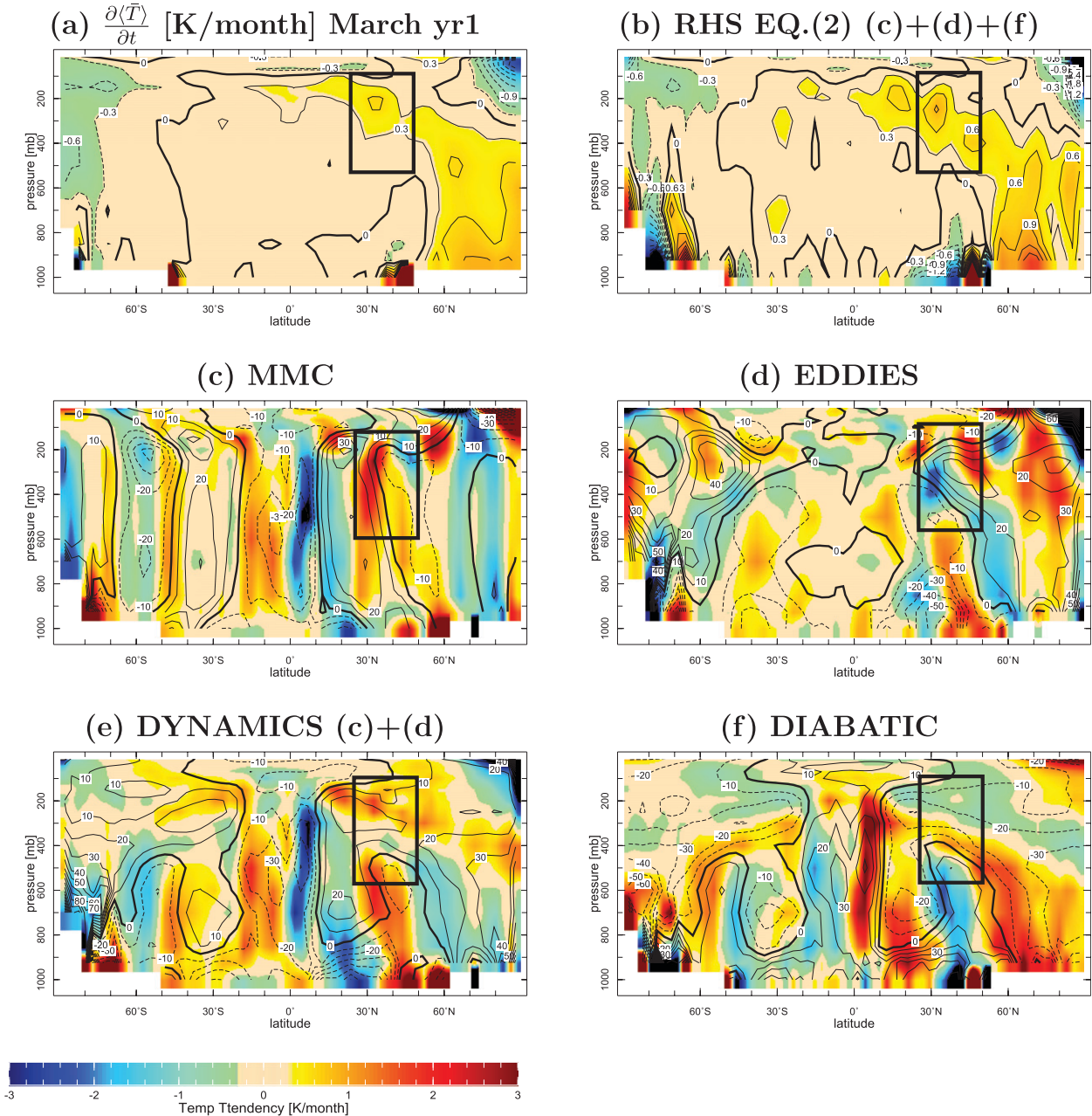


FIG. 9. (a) The actual zonal mean temperature tendency ( $\partial(\bar{T})/\partial t$ ); (b) the temperature tendency in sum of (c)–(f); temperature tendencies due to (c) MMC, (d) total eddies (stationary and transient eddies), and (f) total diabatic heating; and (e) dynamical heating in the sum of (c),(d). The plots are all for March of year 1 and have units of  $\text{K month}^{-1}$ . Both the contours and colors in (a),(b) show the  $2\text{CO}_2$  response with a contour interval of  $0.3 \text{ K month}^{-1}$ . The colors in (c)–(f) show the  $2\text{CO}_2$  response, while the contours show the climatology.

*d. Possible dynamical mechanisms*

Based on the above diagnostic work, we propose a possible dynamical mechanism for the extratropical circulation response to increased  $\text{CO}_2$  with the following sequence:

- 1) The  $\text{CO}_2$  doubling gives rise to a westerly zonal wind anomaly in the stratosphere. The westerly acceleration propagates downward into the lower stratosphere and upper troposphere.
- 2) The westerly acceleration in the lower stratosphere and upper troposphere changes the propagation of

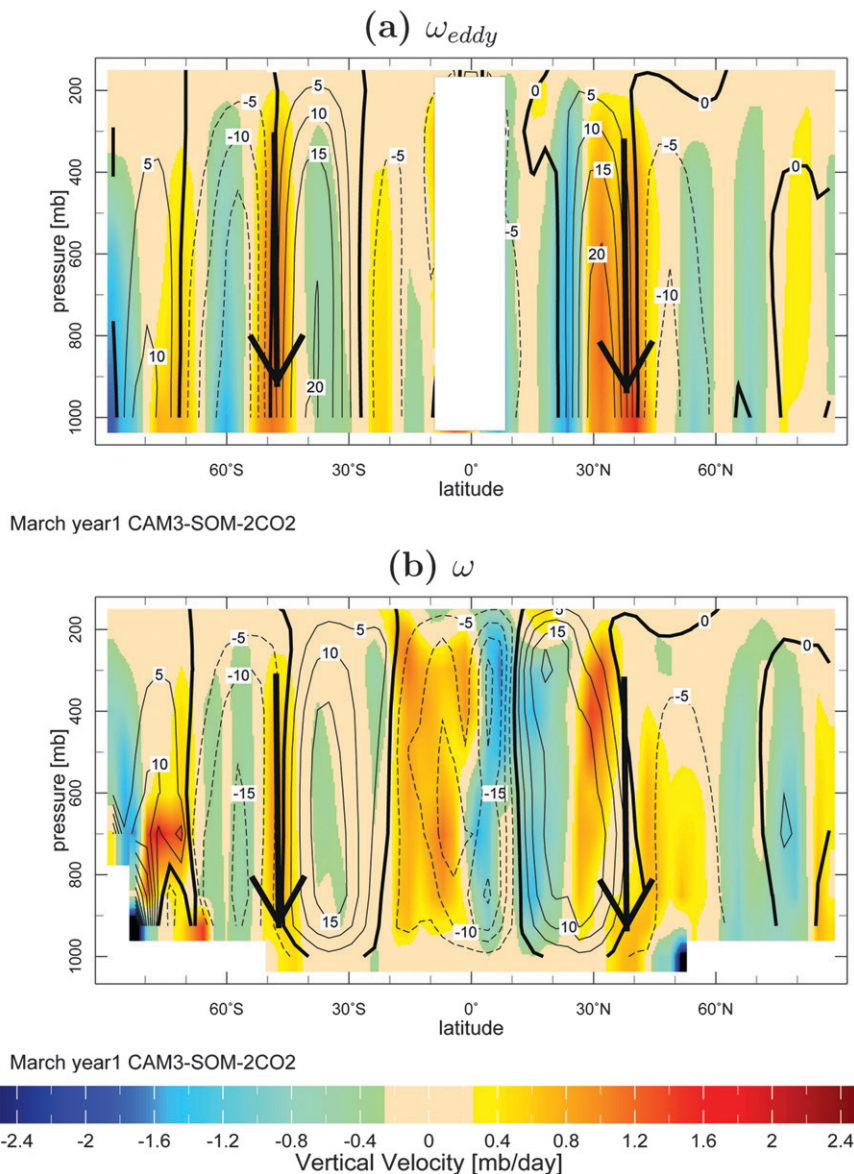
March year1 CAM3-SOM-2CO<sub>2</sub>

FIG. 10. (a) The transient  $\omega_{\text{eddy}}$  ( $\text{mb day}^{-1}$ ) and (b) the actual vertical motion  $\omega$  ( $\text{mb day}^{-1}$ ) from model output in March of year 1. Equation (3) for eddy-driven vertical motion is not applicable in the deep tropics, and thus regions between  $10^{\circ}\text{S}$  and  $10^{\circ}\text{N}$  are masked out in (a). The colors show the  $2\text{CO}_2$  response, while the contours show the climatological results with a contour interval of  $5 \text{ mb day}^{-1}$ . The positive (negative) values in  $\omega_{\text{eddy}}$  ( $\omega$ ) denote downward (upward) motion.

- baroclinic eddies, leading to enhanced transient eddy momentum flux convergence between  $40^{\circ}\text{N(S)}$  and  $60^{\circ}\text{N(S)}$ .
- 3) The increased transient eddy momentum flux convergence drives an anomalous mean meridional circulation in the troposphere as well as a poleward displacement of the tropospheric jets.
  - 4) The induced anomalous descending motion in the subtropical mid- and upper troposphere leads to an adiabatic heating anomaly and thus a broad warming expansion beyond the tropical convective region. The subtropical warming allows for adjustment to the thermal wind balance with the poleward-shifted jets.

A schematic figure showing the hypothesized sequence of the dynamical response is shown in Fig. 11. Other mechanisms are also possible. For example, it is expected that the increase in tropopause height could cause an increase in the length scale of transient eddies, which has been associated with a poleward jet shift (Williams 2006). The dynamical mechanisms of the transient adjustment and their cause and effect, explaining all possibilities, will be analyzed in detail in Part II. Here we provide a brief summary of Part II. Part II will emphasize the transient sequential response in both the stratosphere and the troposphere before the circulation change is well established in the extratropical troposphere. Three phases are defined during the period of transient adjustment. A fast, radiatively induced thermal response occurs during January (defined as phase 1) and an easterly anomaly is generated in the NH subpolar stratosphere. Phase 2, which covers February, features a westerly acceleration in the stratosphere, and this is driven dynamically by the intensified momentum flux convergence of planetary stationary eddies. A “downward propagation” of the westerly acceleration from the lower stratosphere to the troposphere is seen in March and April (phase 3), and this is followed by a poleward displacement of the tropospheric midlatitude jets. In this final phase, the transient eddies play an important role in shifting the position of the tropospheric zonal wind.

#### 4. Eddy-driven vertical motion in CMIP3–IPCC AR4 coupled models

The work so far has demonstrated the importance of the eddy-driven vertical motion in inducing the warming anomaly in the mid- and upper troposphere from our instantaneous CO<sub>2</sub> doubling experiments in CAM3–SOM. This section extends the work to an ensemble of CMIP3–IPCC AR4 coupled models (Meehl et al. 2007b) and shows that the above conclusions also apply in these models. Because the CMIP3–IPCC AR4 Special Report on Emissions Scenarios (SRES) A1B experiments are quasi-equilibrium runs and the diabatic heating term is not available in the standard output, we cannot examine the causality sequence or close the zonal mean temperature equation as in the previous section. Instead, we calculate  $\omega_{\text{eddy}}$  from Eq. (3) using  $\langle \overline{u'v'} \rangle$  from the model output and compare it to the total vertical motion  $\omega$ . Table 1 lists the 14 models used in this analysis. These models are chosen based on the availability of daily variables for both the Twentieth-Century Climate in Coupled Model (20C3M) runs (1961–2000) and the SRES A1B runs (2081–2100). They are the same models analyzed in Seager et al. (2010c), except for the Institute of Numerical Mathematics Coupled Model, version 3.0

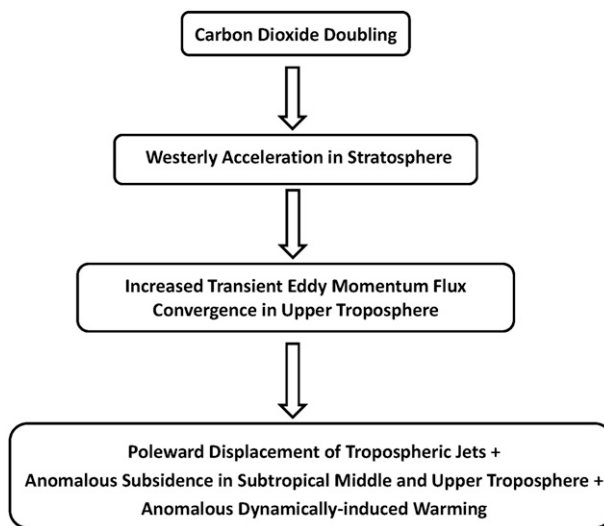


FIG. 11. Summary of the proposed mechanisms causing the tropospheric extratropical circulation response to increased CO<sub>2</sub> concentration.

(INM-CM3.0), which has no available output for 2081–2100. The late twenty-first-century trend is defined as the difference between 2081 and 2100 and 1961 and 2000.

Figure 12 shows the multimodel annual average of  $\langle \overline{T} \rangle$ ,  $\langle \overline{u} \rangle$ ,  $\langle \overline{u'v'} \rangle$ ,  $\langle \overline{u_H v_H} \rangle$ ,  $\langle \overline{\omega}_{\text{eddy}} \rangle$ , and  $\langle \overline{\omega} \rangle$  for the 1961–2000 climatology (shown in black contours) and the late twenty-first century trend (shown in colors) in the troposphere from 200<sup>6</sup> to 1000 mb. The high-pass filter again retains the variability of a time scale of 2–8 days. As is expected, there is a broad temperature increase in the whole troposphere. For example, the 4-K temperature increase extends to about 40°S and 50°N. Both the tropospheric jets and (high frequency) transient eddy momentum flux shift poleward with an intensification on the poleward flank. There is also an anomalous downward motion in the subtropics between 30°N(S) and 50°N(S). The agreement between  $\omega_{\text{eddy}}$  and  $\omega$  in both the location and amplitude supports the idea that the descending motion anomaly is driven by the enhanced transient eddy momentum flux convergence, primarily via the high-frequency component. This is a robust feature for each of these 14 models except for the Institute of Atmospheric Physics Flexible Global Ocean–Atmosphere–Land System Model (IAP FGOALS). Therefore, the linkage between the eddy-driven vertical motion anomaly and the subtropical warming expansion in the mid- and upper troposphere is consistent with the CAM3–SOM results, although the cause and effect cannot be assessed for the CMIP3–IPCC AR4 models.

<sup>6</sup> Daily atmosphere data are output to standard levels up to 200 mb.

TABLE 1. The 14 IPCC AR4 coupled models and their resolution for the atmospheric component used in this study.

Model	Acronym	Atmospheric resolution
Canadian Centre for Climate Modelling and Analysis Coupled General Circulation Model, version 3.1	CGCM3.1 T47	T47L31
Canadian Centre for Climate Modelling and Analysis Coupled General Circulation Model, version 3.1	CGCM3.1 T63	T63L31
Centre National de Recherches Météorologiques Coupled Global Climate Model, version 3	CNRM-CM3	T63L45
Commonwealth Scientific and Industrial Research Organisation Mark version 3.5	CSIRO Mk3.5	T63L18
Geophysical Fluid Dynamics Laboratory Climate Model version 2.0	GFDL CM2.0	2.5° × 2°L24
Geophysical Fluid Dynamics Laboratory Climate Model version 2.1	GFDL CM2.1	2.5° × 2°L24
Goddard Institute for Space Studies Atmosphere–Ocean Model	GISS-AOM	4° × 3°L12
Goddard Institute for Space Studies Model E-R	GISS-ER	5° × 4°L20
Institute of Atmospheric Physics Flexible Global Ocean–Atmosphere–Land System Model	IAP FGOALS	T42L26
L’Institut Pierre-Simon Laplace Coupled Model, version 4A	IPSL CM4A	2.5° × 3.75°L19
Meteorological Institute of the University of Bonn, ECHO-G Model	MIUBECHOG	T30L19
Model for Interdisciplinary Research on Climate 3.2, medium-resolution version	MIROC3.2(medres)	T42L20
ECHAM5	ECHAM5	T63L31
Meteorological Research Institute Coupled General Circulation Model, version 2.3.2a	MRI CGCM2.3	T42L30

## 5. Discussions and conclusions

We have explored the transient evolution of the atmospheric adjustment to an instantaneous doubling of CO<sub>2</sub> concentration. The sequence in the general circulation response in the atmosphere helps reveal the dynamical mechanisms underlying the equilibrium circulation response, for example, the poleward expansion of the Hadley Cell (Lu et al. 2007), and the poleward shift of the tropospheric jets and storm tracks (e.g., Kushner et al. 2001; Yin 2005), as found in CMIP3–IPCC AR4 models. In contrast to previous studies suggesting that the thermal forcing in the tropical upper troposphere drives the tropospheric circulation response (e.g., Butler et al. 2010), our results indicate that the broad warming expansion in the subtropical mid- and upper troposphere is a consequence of the circulation change. Enhanced transient eddy momentum flux convergence in the lower stratosphere and upper troposphere, possibly originating from the stratospheric westerly acceleration, drives an anomalous mean meridional circulation in the troposphere. The induced anomalous descending motion in the subtropical mid- and upper troposphere warms the air adiabatically. Afterward, the subtropical warming and the poleward displacement of the jets and the baroclinic eddies can potentially feedback positively onto each other via a poleward shift in the eddy generation region, leading to a further poleward shift of the jets and the eddies and a further warming expansion in the subtropical troposphere.

It is noted here that this study focuses primarily on the atmospheric transient adjustment process before there is any appreciable SST change. Certainly SST change in a longer time scale may cause further circulation change.

Nonetheless, the transient adjustment shown here is similar to the results in CMIP3–IPCC AR4 fully coupled models. As also demonstrated in Lu et al. (2009), the observed widening of the tropics in the latter half of the twentieth century is entirely attributed to the direct effect in the atmosphere of changing trace gas concentrations rather than to SST warming.

Our results also show the sequence of the zonal wind anomaly in the vertical column of the atmosphere, indicating that the poleward displacement of the tropospheric jets follows the subpolar westerly anomaly in the stratosphere. It suggests the importance of the stratosphere, and the coupling between the stratosphere and the troposphere, in regulating the extratropical tropospheric circulation response to increasing CO<sub>2</sub>. A detailed analysis of the stratospheric response and the stratosphere–troposphere coupling, including how the response “migrates” downward into the troposphere and how the eddies respond step by step, will be further examined in Part II. It is noted here that our study intends to understand the circulation response and the dynamical mechanisms in CMIP3–IPCC AR4–like models, albeit most of the models have poorly resolved stratospheres. Some studies have argued that a well-resolved stratosphere is required to reproduce observed behavior (e.g., Shindell et al. 1999; Sassi et al. 2010). However, Sigmond et al. (2008) suggested that the atmospheric circulation response to CO<sub>2</sub> doubling does not necessarily require a well-resolved stratosphere, but rather a realistic simulation of the zonal wind strength in the mid- and high-latitude lower stratosphere. The zonal mean zonal wind in CAM3 agrees with the reanalysis data in this region. The circulation response to a CO<sub>2</sub> doubling in both the troposphere and the stratosphere in our results also agrees

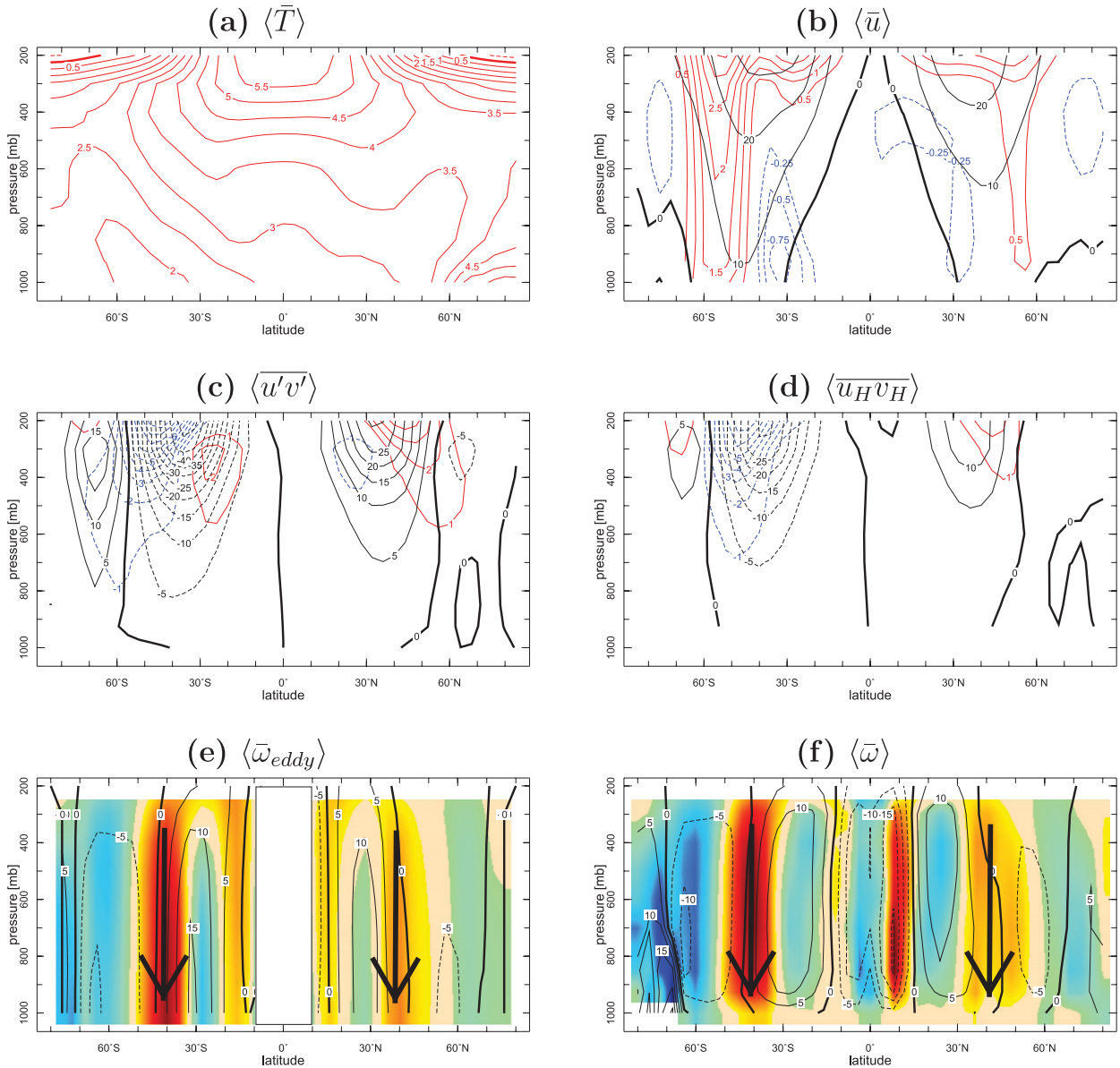


FIG. 12. The late twenty-first-century trend in annual mean (a)  $\langle \bar{T} \rangle$  (K), (b)  $\langle \bar{u} \rangle$  ( $\text{m s}^{-1}$ ), (c)  $\langle \overline{u'v'} \rangle$  ( $\text{m}^2 \text{s}^{-2}$ ), (d)  $\langle \overline{u_H v_H} \rangle$  ( $\text{m}^2 \text{s}^{-2}$ ), (e)  $\langle \bar{\omega}_{\text{eddy}} \rangle$  ( $\text{mb day}^{-1}$ ), and (f)  $\langle \bar{\omega} \rangle$  ( $\text{mb day}^{-1}$ ) averaged in 14 MIP3-IPCC AR4 coupled models. The color contours (shadings) show the difference between 2081 and 2100 (SRES A1B) and 2000, while the black contours show the average of 1961–2000. The color scale in (e),(f) is as in Fig. 10. It is noted that the pressure level is up to 200 mb due to the availability of daily variables.

to a large extent with those from studies that used models with much finer vertical resolution in the middle atmosphere (e.g., Shindell et al. 2001; Sigmond et al. 2004). However, a model lid in the midstratosphere is known to impact the vertical propagation of stationary planetary scale waves during NH winter (Shaw and Perlwitz 2010; Sassi et al. 2010). Assessing the transient and equilibrium responses to  $\text{CO}_2$  doubling in a model with high vertical resolution and a high model lid height is the subject of future investigation. Finally, because

our experiments double the  $\text{CO}_2$  concentration on 1 January, it would be interesting to change the time of  $\text{CO}_2$  doubling to see if the model responds differently. A set of experiments with an instantaneous  $\text{CO}_2$  doubling on 1 July is currently under investigation.

*Acknowledgments.* The authors greatly appreciate the useful views of two anonymous reviewers and Dr. Joe Kidston. We would also like to thank the Global Decadal Hydroclimate (GloDecH) group at Lamont-Doherty

Earth Observatory and Columbia University for their comments and advice, in particular, Prof. Lorenzo Polvani and Dr. Michela Biasutti as well as Dr. Nili Harnik. We also thank Profs. Ngar-Cheung Lau, Geoffrey K. Vallis, and Benjamin Lintner for the helpful discussions. YW was supported by NASA headquarters under the NASA Earth and Space Science Fellowship Program Grant NNX08AU80H. RS, MT, and NN were supported by NOAA Awards NA08OAR4320912 and NA10OAR4320137, and NSF Awards ATM-0804107. TAS was supported by a postdoctoral fellowship from the Natural Sciences and Engineering Research Council of Canada.

## REFERENCES

- Baldwin, M. P., and T. J. Dunkerton, 2001: Stratospheric harbingers of anomalous weather regimes. *Science*, **294**, 581–584.
- Boville, B. A., and C. S. Bretherton, 2003: Heating and kinetic energy dissipation in the NCAR Community Atmosphere Model. *J. Climate*, **16**, 3877–3887.
- Butler, A. H., D. W. J. Thompson, and R. Heikes, 2010: The steady-state atmospheric circulation response to climate change–like thermal forcings in a simple general circulation model. *J. Climate*, **23**, 3474–3496.
- Chen, G., and I. M. Held, 2007: Phase speed spectra and the recent poleward shift of Southern Hemisphere surface westerlies. *Geophys. Res. Lett.*, **34**, L21805, doi:10.1029/2007GL031200.
- Collins, W. D., and Coauthors, 2004: Description of the NCAR Community Atmosphere Model (CAM3.0). NCAR Tech. Note NCAR/TN-464+STR, 226 pp.
- , and Coauthors, 2006: The formulation and atmospheric simulation of the Community Atmosphere Model Version 3 (CAM3). *J. Climate*, **19**, 2144–2161.
- Gregory, J. M., and M. Webb, 2008: Tropospheric adjustment induces a cloud component in CO<sub>2</sub> forcing. *J. Climate*, **21**, 58–71.
- , and Coauthors, 2004: A new method for diagnosing radiative forcing and climate sensitivity. *Geophys. Res. Lett.*, **31**, L03205, doi:10.1029/2003GL018747.
- Hansen, J., A. Lacis, D. Rind, G. Russell, P. Stone, I. Fung, R. Ruedy, and J. Lerner, 1984: Climate sensitivity: Analysis of feedback mechanisms. *Climate Processes and Climate Sensitivity*, *Geophys. Monogr.*, Vol. 29, Amer. Geophys. Union, 130–163 pp.
- Harnik, N., R. Seager, N. Naik, M. Cane, and M. Ting, 2010: The role of linear wave refraction in the transient eddy–mean flow response to tropical Pacific SST anomalies. *Quart. J. Roy. Meteor. Soc.*, **136**, 2132–2146, doi:10.1002/qj.688.
- Haynes, P. H., M. E. McIntyre, T. G. Shepherd, C. J. Marks, and K. P. Shine, 1991: On the downward control of extratropical diabatic circulations by eddy-induced mean zonal forces. *J. Atmos. Sci.*, **48**, 651–678.
- Held, I. M., 1993: Large-scale dynamics and global warming. *Bull. Amer. Meteor. Soc.*, **74**, 228–241.
- , and B. J. Soden, 2006: Robust response of the hydrological cycle to global warming. *J. Climate*, **19**, 5686–5699.
- Hu, Y., and Q. Fu, 2007: Observed poleward expansion of the Hadley circulation since 1979. *Atmos. Chem. Phys.*, **7**, 5229–5236.
- Hurrell, J. W., J. J. Hack, A. S. Phillips, J. Caron, and J. Yin, 2006: The dynamical simulation of the Community Atmosphere Model version 3 (CAM3). *J. Climate*, **19**, 2162–2183.
- Kidston, J., S. M. Dean, J. Renwick, and G. K. Vallis, 2010: A robust increase in the eddy length scale in the simulation of future climates. *Geophys. Res. Lett.*, **37**, L03806, doi:10.1029/2009GL041615.
- , G. K. Vallis, S. M. Dean, and J. A. Renwick, 2011: Can the increase in the eddy length scale under global warming cause the poleward shift of the jet streams? *J. Climate*, **24**, 3764–3780.
- Kushner, P. J., I. M. Held, and T. L. Delworth, 2001: Southern Hemisphere atmospheric circulation response to global warming. *J. Climate*, **14**, 2238–2249.
- Lorenz, D. J., and E. T. DeWeaver, 2007: Tropopause height and zonal wind response to global warming in the IPCC scenario integrations. *J. Geophys. Res.*, **112**, D10119, doi:10.1029/2006JD008087.
- Lu, J., G. A. Vecchi, and T. Reichler, 2007: Expansion of the Hadley cell under global warming. *Geophys. Res. Lett.*, **34**, L06805, doi:10.1029/2006GL028443.
- , G. Chen, and D. M. W. Frierson, 2008: Response of the zonal mean atmospheric circulation to El Niño versus global warming. *J. Climate*, **21**, 5835–5851.
- , C. Deser, and T. Reichler, 2009: Cause of the widening of the tropical belt since 1958. *Geophys. Res. Lett.*, **36**, L03803, doi:10.1029/2008GL036076.
- Manabe, S., K. Bryan, and M. J. Spelman, 1990: Transient response to a global ocean–atmosphere model to a doubling of atmosphere carbon dioxide. *J. Phys. Oceanogr.*, **20**, 722–749.
- McCaa, J. R., M. Rothstein, B. E. Eaton, J. M. Rosinski, E. Kluzek, and M. Vertenstein, 2004: User’s guide to the NCAR Community Atmosphere Model (CAM 3.0). NCAR Tech. Rep., 85 pp.
- McLandress, C., T. G. Shepherd, J. F. Scinocca, D. A. Plummer, M. Sigmon, A. I. Jonsson, and M. C. Reader, 2011: Separating the dynamical effects of climate change and ozone depletion. Part II: Southern Hemisphere troposphere. *J. Climate*, **24**, 1850–1868.
- Meehl, G. A., and W. M. Washington, 1996: El Niño-like climate change in a model with increased atmospheric CO<sub>2</sub> concentrations. *Nature*, **382**, 56–60.
- , and Coauthors, 2007a: Global climate projections. *Climate Change 2007: The Physical Science Basis*, S. Solomon et al., Eds., Cambridge University Press, 747–845.
- , C. Covey, T. Delworth, M. Latif, B. McAvaney, J. F. B. Mitchell, R. J. Stouffer, and K. E. Taylor, 2007b: WCRP CMIP3 multimodel dataset: A new era in climate change research. *Bull. Amer. Meteor. Soc.*, **88**, 1383–1394.
- O’Gorman, P. A., 2010: Understanding the varied response of the extratropical storm tracks to climate change. *Proc. Natl. Acad. Sci. USA*, **107**, 19 176–19 180.
- Polvani, L., D. Waugh, G. Correa, and S.-W. Son, 2011: Stratospheric ozone depletion: The main driver of twentieth-century atmospheric circulation changes in the Southern Hemisphere. *J. Climate*, **24**, 795–812.
- Rasch, P. J., and Coauthors, 2006: A characterization of tropical transient activity in the CAM3 atmospheric hydrologic cycle. *J. Climate*, **19**, 2222–2242.
- Reichler, T., M. Dameris, and R. Sausen, 2003: Determining the tropopause height from gridded data. *Geophys. Res. Lett.*, **30**, 2042, doi:10.1029/2003GL018240.
- Sassi, F., R. R. Garcia, D. Marsh, and K. W. Hoppel, 2010: The role of the middle atmosphere in simulations of the troposphere during Northern Hemisphere winter: Differences between high- and low-top models. *J. Atmos. Sci.*, **67**, 3048–3064.

- Seager, R., and N. Naik, 2012: A mechanisms-based approach to detecting recent anthropogenic hydroclimate change. *J. Climate*, **25**, 236–261.
- , N. Harnik, Y. Kushnir, W. Robinson, and J. Miller, 2003: Mechanisms of hemispherically symmetric climate variability. *J. Climate*, **16**, 2960–2978.
- , and Coauthors, 2009: Mexican drought: An observational modeling and tree ring study of variability and climate change. *Atmósfera*, **22**, 1–31.
- , N. Naik, W. Baethgen, A. Robertson, Y. Kushnir, J. Nakamura, and S. Jurburg, 2010a: Tropical oceanic causes of interannual to multidecadal precipitation variability in southeast South America over the past century. *J. Climate*, **23**, 5517–5539.
- , —, M. Ting, M. A. Cane, N. Harnik, and Y. Kushnir, 2010b: Adjustment of the atmospheric circulation to tropical Pacific SST anomalies: Variability of transient eddy propagation in the Pacific–North America sector. *Quart. J. Roy. Meteor. Soc.*, **136**, 277–296, doi:10.1002/qj.588.
- , —, and G. A. Vecchi, 2010c: Thermodynamic and dynamic mechanisms for large-scale changes in the hydrological cycle in response to global warming. *J. Climate*, **23**, 4651–4668.
- Shaw, T. A., and J. Perlwitz, 2010: The impact of stratospheric model configuration on planetary-scale waves in Northern Hemisphere winter. *J. Climate*, **23**, 3369–3389.
- Shindell, D. T., R. L. Miller, G. A. Schmidt, and L. Pandolfo, 1999: Simulation of recent northern winter climate trends by greenhouse-gas forcing. *Nature*, **399**, 452–455.
- , G. A. Schmidt, R. L. Miller, and D. Rind, 2001: Northern Hemisphere winter climate response to greenhouse gas, ozone, solar, and volcanic forcing. *J. Geophys. Res.*, **106**, 7193–7210, doi:10.1029/2000JD900547.
- Sigmond, M., P. C. Siegmund, E. Manzini, and H. Kelder, 2004: A simulation of the separate climate effects of middle-atmospheric and tropospheric CO<sub>2</sub> doubling. *J. Climate*, **17**, 2352–2367.
- , J. F. Scinocca, and P. J. Kushner, 2008: Impact of the stratosphere on tropospheric climate change. *Geophys. Res. Lett.*, **35**, L12706, doi:10.1029/2008GL033573.
- Vecchi, G. A., and B. J. Soden, 2007: Global warming and the weakening of the tropical circulation. *J. Climate*, **20**, 4316–4340.
- Williams, G. P., 2006: Circulation sensitivity to tropopause height. *J. Atmos. Sci.*, **63**, 1954–1961.
- Wu, Y., M. Ting, R. Seager, H.-P. Huang, and M. A. Cane, 2010: Changes in storm tracks and energy transports in a warmer climate simulated by the GFDL CM2.1 model. *Climate Dyn.*, **37**, 53–72, doi:10.1007/s00382-010-0776-4.
- Yin, J. H., 2005: A consistent poleward shift of the storm tracks in simulations of 21st century climate. *Geophys. Res. Lett.*, **32**, L18701, doi:10.1029/2005GL023684.